AIAA 2003-0974

The Langley Stability and Transition Analysis Code (LASTRAC) : LST, Linear & Nonlinear PSE for 2-D, Axisymmetric, and Infinite Swept Wing Boundary Layers

Chau-Lyan Chang
NASA Langley Research Center
Hampton, VA

41st AIAA Aerospace Sciences Meeting & Exhibit
6-9 January 2003
Reno, Nevada

The Langley Stability and Transition Analysis Code (LASTRAC) : LST, Linear & Nonlinear PSE for 2-D, Axisymmetric, and Infinite Swept Wing Boundary Layers

Chau-Lyan Chang *
NASA Langley Research Center
MS 128
Hampton, VA 23681
c.chang@larc.nasa.gov

Abstract

During the past two decades, our understanding of laminar-turbulent transition flow physics has advanced significantly owing to, in a large part, the NASA program support such as the National Aerospace Plane (NASP), High-speed Civil Transport (HSCT), and Advanced Subsonic Technology (AST). Experimental, theoretical, as well as computational efforts on various issues such as receptivity and linear and nonlinear evolution of instability waves take part in broadening our knowledge base for this intricate flow phenomenon. Despite all these advances, transition prediction remains a nontrivial task for engineers due to the lack of a widely available, robust, and efficient prediction tool. The design and development of the LASTRAC code is aimed at providing one such engineering tool that is easy to use and yet capable of dealing with a broad range of transition related issues. LASTRAC was written from scratch based on the state-of-the-art numerical methods for stability analysis and modern software technologies. At low fidelity, it allows users to perform linear stability analysis and N-factor transition correlation for a broad range of flow regimes and configurations by using either the linear stability theory (LST) or linear parabolized stability equations (LPSE) method. At high fidelity, users may use nonlinear PSE to track finite-amplitude disturbances until the skin friction rise. Coupled with the built-in receptivity model that is currently under development, the nonlinear PSE method offers a synergistic approach to predict transition onset for a given disturbance environment based on first principles. This paper describes the governing equations, numerical methods, code development, and case studies for the current release of LASTRAC. Practical applications of LASTRAC are demonstrated for linear stability calculations, N-factor transition correlation, nonlinear breakdown simulations, and controls of stationary crossflow instability in supersonic swept wing boundary layers.

Introduction

In the late 80's till the early 90's, laminar-turbulent transition research was one of the outstanding issues for the National Aerospace Plane (NASP), High Speed Research (HSR), and Advanced Subsonic Technology (AST) programs. After a dormant period, there has been renewed interest in supersonic laminar flow aircraft in recent years due to the DARPA Quiet Supersonic Platform (QSP) project. The main objective of the QSP project is to evaluate the feasibility of a low-boom laminar flow supersonic aircraft.[1] The ongoing NASA Langley Supersonic Vehicle Technology (SVT) program is also aimed at developing technologies required for designing such supersonic vehicles. Computational tool development as well as a series of wind-tunnel and flight experiments are planned.

Laminar flow control has been investigated extensively over the past decades. Experimental, theoretical, as well as computational efforts on various issues such as receptivity, linear and nonlinear evolution of instability waves take part in broadening our knowledge base of this intricate flow phenomenon. For low speed flows, various stages of the transition process are now fairly well understood. Theory and numerical simulations using either parabolized stability equations (PSE) or direct numerical simulations (DNS) accurately describe disturbance generation and evolution until the transitional stage. Secondary instability in two-dimensional and swept wing boundary layers observed in low-speed experiments may also be calculated accurately using nonlinear PSE and the eigenvalue approach.[2,3] Saric et al.[4] discovered that stationary crossflow instability can be controlled by introducing distributed roughness near the leading edge to alter the mean state and subsequently suppress or delay the growth of the most unstable disturbances. It has been shown that this control phenomenon may be calculated and parametrically studied by nonlinear PSE (see Malik et al.[3] and Chang[5]).

For supersonic to hypersonic boundary layers, the breakdown mechanism is not fully understood largely due to the lack of experimental measurements. For two-dimensional boundary layers, it has been shown computationally that the secondary instability mechanism observed in low speed cases may still be present.[2] But other mechanisms, such as oblique-mode breakdown (Chang & Malik[6]), may be more relevant because of the large growth of the oblique disturbances in low supersonic boundary layers. At hy-

*Senior Member, AIAA. Research Scientist NASA LaRC

personic speed, large amplitude second-mode disturbances have been observed experimentally[7,8] but the breakdown mechanism is unclear, mainly because the wave orientation is largely unknown. The recent experiment of a flared cone in a conventional Mach 6 tunnel by Horvath et al.[9] indicates that transition may or may not be caused by second-mode disturbances because of a small N-factor at the transition onset. We need more detailed experimental measurements to clarify this issue. Receptivity of hypersonic boundary layers to acoustic disturbance has been studied by Federov[10] and Zhong.[11] The role of the entropy layer on hypersonic boundary layers is investigated both theoretically and numerically by Fedorov & Tumin.[12] For supersonic swept wing boundary layers, Saric is currently extending his distributed roughness control for supersonic flows.[13]

Despite all the advances in transition research, the traditional way of transition correlation and prediction using the e^N method remains one of the mainstream tools used in the design phase due to its simplicity and availability. The N-factor method provides a simple way to correlate transition locations and in the meantime predict transition onset using a prescribed N-value. For a higher fidelity transition prediction based on first principles, one can start from the receptivity model and compute the disturbance initial amplitudes according to the given disturbance environment such as a roughness or free-stream disturbance distribution. Receptivity calculations may be based on a simple linear theory or a more advanced linear Navier-Stokes (LNS) method.[14,15] The evolution of the internalized disturbances with known amplitudes can then be calculated using nonlinear PSE all the way until the skin friction rise. Alternatively, a secondary instability calculation may be performed for a steady, highly nonlinear boundary layer with the presence of stationary crossflow vortices.[3] To further refine the transition region or to carry the perturbed field into a fully turbulent stage, DNS or large eddy simulation (LES) may be used.

The integrated transition prediction approach described above encompasses several mature computational means to form a package of tools for high-fidelity predictions beyond the conventional e^N method. Our current research effort is geared toward this integrated approach. In addition to the tool development, at issue is the disturbance environment. A complete description of the environment remains very difficult except for a forced transition where manually excited roughness or free-stream waves outweigh the natural ones and thus may be quantified accurately in the computations. As a result, statistical means must be introduced to account for the natural environment. Some efforts have been made along this direction.[16] A case study for supersonic swept wing using the integrated approach is also available.[17]

One of the main goals of the ongoing NASA Langley projects for transition flow physics and prediction is to devise a set of tools to enable traditional as well as integrated transition prediction. The Langley Stability and Transition Analysis Code (LASTRAC) was developed to meet two main objectives: to provide an easy-to-use engineering tool for routine use and to incorporate state-of-the-art computational and theoretical findings for integrated transition predictions. For the former objective, LASTRAC can perform linear calculations and transition correlation using the N-factor method based on either LST or a more advanced linear PSE method. The user interface of LASTRAC code was designed to allow users to identify unstable parameter space in terms of disturbance frequency and wave numbers with minimum effort. Transition prediction or correlation thus can be made with the identified parameter space. In addition to the traditional LST-based N-factor calculations, LASTRAC allows users to perform linear PSE N-factor calculations, which in some cases give a more compact N-factor range and better correlation.

To achieve the second objective, LASTRAC provides transition simulation capability based on an absolute amplitude. The receptivity module computes the initial amplitudes near the neutral stability location. Nonlinear PSE then simulates disturbance evolution until skin friction rise. For further refinement near the transition region, a sub-grid scale model based nonlinear PSE, or large eddy simulation (LES) and direct numerical simulation (DNS) may be used. These modules are all currently under development. We will discuss mainly the nonlinear PSE method in this paper.

In the current LASTRAC release, LST and linear and nonlinear PSE options are implemented for 2-D, axisymmetric, and infinite swept wing boundary layers. In addition, 2-D mixing layer, axisymmetric jet and vortex flows are also handled by the current release. Extension to general three-dimensional(3-D) boundary layers is currently under development. This paper is a status report of the LASTRAC development. We discuss governing equations, numerical solutions, code development, and case studies of LASTRAC for practical examples in this paper.

Governing Equations

The problem of interest is a compressible flow over a 2-D or axisymmetric body with a coordinate system depicted in Fig.1 where x is the streamwise, y the wall-normal, and z the spanwise direction (or the azimuthal direction for axisymmetric cases). For the case of infinite swept wing boundary layers, the coordinate system used is shown in Fig.2 where x is the normal-chord direction and z is parallel to the leading edge. A nonorthogonal coordinate system can also be used for infinite swept wing boundary layers and will be used for future LASTRAC releases. A body-fitted coordinate is adopted because we are interested in a region adjacent to the wall. For 2-D or axisymmetric configurations, both streamwise curvature along x and transverse curvature along z may be included in the computation; only streamwise curvature is allowed for an infinite swept wing configuration. In the orthogonal body-fitted coordinate system, elements of length are $h_1 dx$, dy, and $h_3 dz$, in the $x-$, $y-$, and z-direction, respectively. The

element length can be written as

$$dl = \sqrt{(h_1 dx)^2 + dy^2 + (h_3 dz)^2}.$$

The metric h_1 is associated with the streamwise curvature κ and is defined as

$$h_1 = 1 + \kappa y.$$

The metric h_3 is unity for nonaxisymmetric bodies; for axisymmetric configurations, it is defined as

$$h_3 = r_b + y\cos(\theta)$$

where r_b is the local radius and θ is local half-angle along the axisymmetric surface.

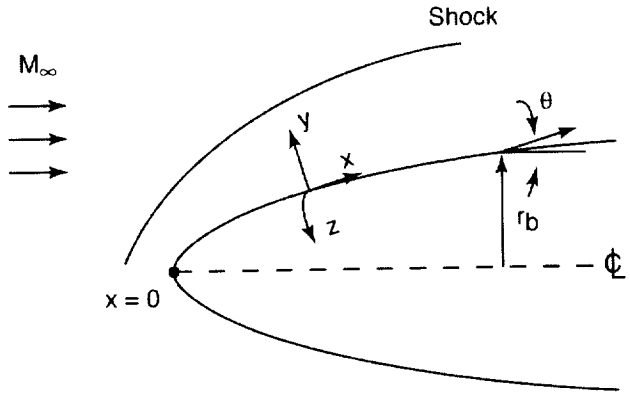

Fig. 1 Coordinate system for a 2-D or axisymmetric boundary layer

The evolution of disturbances is governed by the compressible Navier-Stokes equations

$$\begin{aligned}
\frac{\partial \rho}{\partial t} + \nabla \cdot (\rho \vec{V}) &= 0 \\
\rho[\frac{\partial \vec{V}}{\partial t} + \vec{V} \cdot \nabla)\vec{V}] &= -\nabla p + \nabla[\lambda(\nabla \cdot \vec{V})] \\
&+ \nabla \cdot [\mu(\nabla \vec{V} + \nabla \vec{V}^T)] \quad (1) \\
\rho C_p[\frac{\partial T}{\partial t} + (\vec{V} \cdot \nabla)T] &= \nabla \cdot (k \nabla T) + \frac{\partial p}{\partial t} \\
&+ (\vec{V} \cdot \nabla)p + \Phi
\end{aligned}$$

where $\vec{V}$ is the velocity vector, ρ the density, p the pressure, T the temperature, C_p the specific heat, k the thermal conductivity, and μ and λ the first and second coefficient of viscosity, respectively. The viscous dissipation function is defined as

$$\Phi = \lambda(\nabla \cdot \vec{V})^2 + \frac{\mu}{2}[\nabla \vec{V} + \nabla \vec{V}^T]^2. \quad (2)$$

The second viscosity is related to the first one by the Stokes parameter s, defined as

$$\lambda = \frac{2}{3}(s - 1)\mu. \quad (3)$$

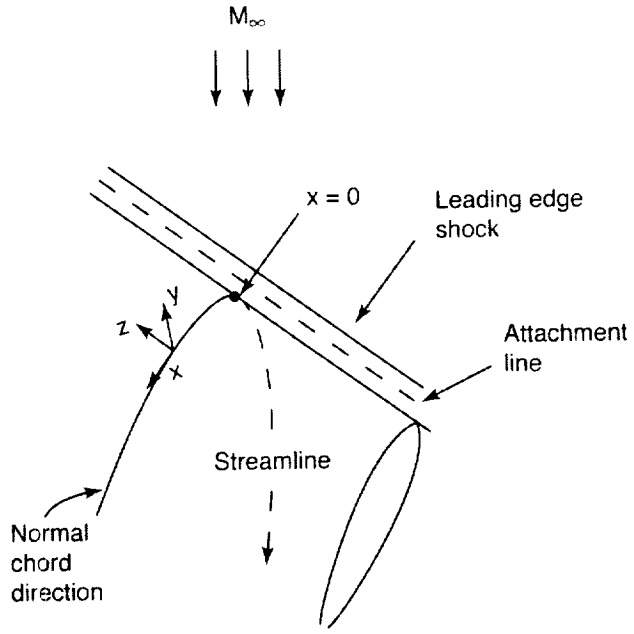

Fig. 2 Coordinate system for an infinite swept wing boundary layer

The perfect gas relation,

$$p = \rho \Re T, \quad (4)$$

is used as the equation of state.

Equation 1 is in a nondimensional form, i.e., all lengths are scaled by a reference length scale ℓ, velocity by u_e, density by ρ_e, pressure by $\rho_e u_e^2$, temperature by T_e, viscosity by μ_e, and time by ℓ/u_e. For stability calculations, these normalization quantities are taken to be the boundary-layer edge values. The length scale ℓ is the similarity boundary-layer length scale defined by

$$\ell = \sqrt{\nu_e x / u_e}, \quad (5)$$

and the corresponding Reynolds number is defined by

$$R = u_e \ell / \nu_e. \quad (6)$$

The solution to the Navier-Stokes equations consists of two parts, the mean laminar flow solution and the disturbance fluctuation, i.e.,

$$\begin{aligned}
u = \bar{u} + u', v = \bar{v} + v', w = \bar{w} + w' \\
p = \bar{p} + p', \rho = \bar{\rho} + \rho', T = \bar{T} + T' \\
\mu = \bar{\mu} + \mu', \lambda = \bar{\lambda} + \lambda', k = \bar{k} + k'.
\end{aligned} \quad (7)$$

Substituting Eq.7 into Eq.1 and subtracting the governing equations for the steady-state basic flow, we obtain the governing equations for the disturbances as

$$\Gamma \frac{\partial \phi}{\partial t} + \frac{A}{h_1}\frac{\partial \phi}{\partial x} + B\frac{\partial \phi}{\partial y} + \frac{C}{h_3}\frac{\partial \phi}{\partial z} + D\phi =$$

$$\frac{1}{R_0}\left(\frac{V_{xx}}{h_1^2}\frac{\partial^2\phi}{\partial x^2}+\frac{V_{xy}}{h_1}\frac{\partial^2\phi}{\partial x\partial y}+V_{yy}\frac{\partial^2\phi}{\partial y^2}\right.$$
$$\left.+\frac{V_{xz}}{h_3}\frac{\partial^2\phi}{\partial x\partial z}+\frac{V_{yz}}{h_3}\frac{\partial^2\phi}{\partial y\partial z}+\frac{V_{zz}}{h_3^2}\frac{\partial^2\phi}{\partial z^2}\right) \quad (8)$$

where ϕ is the disturbance vector defined as

$$\phi=(p',u',v',w',T')^T. \quad (9)$$

The coefficient matrices, Γ, A, B, C, D, V_{xx}, V_{xy}, etc. are the Jacobians of the flux vectors, and $R_0=u_e\ell_0/\nu_e$ is the Reynolds number used to normalize the equations. The reference length scale ℓ_0 depends on the flow configuration. For a boundary-layer flow, the boundary-layer length scale (defined in Eq.5) computed at the initial location of the stability calculations is used. For a jet or shear layer, the jet diameter or shear layer thickness may be used.

The Jacobian matrices can be further decomposed into two parts. The first part contains only mean quantities and the second part contains perturbation quantities. For example,

$$A=A^l+A^n$$

where $A^l = A^l(\bar{p},\bar{u},\bar{v},\bar{w},\bar{T},...)$ and $A^n = A^n(\bar{p},\bar{u},...p',u',...)$.

For a 2-D or infinite swept boundary layer, we assume the disturbance field is periodic in both temporal and spanwise directions. The disturbance vector ϕ can then be expressed as the following discrete Fourier series:

$$\phi(x,y,z,t)=\sum_{m=-M}^{M}\sum_{n=-N}^{N}\chi_{mn}(x,y)e^{i(n\beta z-m\omega t)} \quad (10)$$

where ω and β are the fundamental temporal and spanwise wave number of interest, respectively. M and N are the number of Fourier modes included in the calculation in time and space. The wave number ω is related to the physical frequency f by

$$\omega=\frac{2\pi\ell}{u_e}f. \quad (11)$$

Another nondimensional frequency often used in stability calculations is defined by

$$F=\frac{2\pi\nu_e}{u_e^2}f. \quad (12)$$

The spanwise wave number is defined by

$$\beta=2\pi/\lambda_z \quad (13)$$

where λ_z is the spanwise wavelength normalized by the length scale ℓ_0. The fundamental mode (ω,β) determines the size of the computational domain($1/f$ in time and λ_z in the spanwise direction) and M and N represent the numerical resolution ($2M+1$ and $2N+1$ discretized points in time and the spanwise direction) in the simulation. The mode shape of a mode (m,n) is represented by the complex vector χ_{mn}.

Equation 8 is the governing equation for the disturbance evolution. Direct solution of Eq.8 is referred to as the direct numerical simulation (DNS) method. DNS requires a significant amount of computational time even for a simple linear case. Hence, a more efficient approximate solution to Eq.8 is more desirable. When the disturbance amplitude is very small relative to the mean quantities, each Fourier mode evolves independently. Nonlinear interaction among disturbance modes is negligible. The linearized version of Eq.8 can be written as

$$\Gamma^l\frac{\partial\phi}{\partial t}+\frac{A^l}{h_1}\frac{\partial\phi}{\partial x}+B^l\frac{\partial\phi}{\partial y}+\frac{C^l}{h_3}\frac{\partial\phi}{\partial z}+D^l\phi=$$
$$\frac{1}{R_0}\left(\frac{V_{xx}^l}{h_1^2}\frac{\partial^2\phi}{\partial x^2}+\frac{V_{xy}^l}{h_1}\frac{\partial^2\phi}{\partial x\partial y}+V_{yy}^l\frac{\partial^2\phi}{\partial y^2}\right. \quad (14)$$
$$\left.+\frac{V_{xz}^l}{h_3}\frac{\partial^2\phi}{\partial x\partial z}+\frac{V_{yz}^l}{h_3}\frac{\partial^2\phi}{\partial y\partial z}+\frac{V_{zz}^l}{h_3^2}\frac{\partial^2\phi}{\partial z^2}\right).$$

For a single disturbance mode (ω,β), ϕ can be expressed as

$$\phi=\chi(x,y)e^{i(\beta z-\omega t)}. \quad (15)$$

Substitute the above equation into Eq.14, we obtain

$$\left(\frac{A^l}{h_1}-\frac{i\beta V_{xz}^l}{h_3R_0}\right)\frac{\partial\chi}{\partial x}+\left(B^l+\frac{i\beta V_{yz}^l}{h_3R_0}\right)\frac{\partial\chi}{\partial y}$$
$$+\left(D^l-i\omega\Gamma^l+\frac{i\beta C^l}{h_3}+\frac{\beta^2V_{zz}^l}{h_3^2R_0}\right)\chi= \quad (16)$$
$$\frac{1}{R_0}\left(\frac{V_{xx}^l}{h_1^2}\frac{\partial^2\chi}{\partial x^2}+\frac{V_{xy}^l}{h_1}\frac{\partial^2\chi}{\partial x\partial y}+V_{yy}^l\frac{\partial^2\chi}{\partial y^2}\right).$$

Eq.16 is the linearized Navier-Stokes (LNS) equation, which is a set of constant coefficient PDE's. Solution of the LNS still requires a significant amount of computational time. To further reduce it, approximations to Eq.16 must be made.

In the PSE approach, as suggested by Herbert[18] and Chang et al.,[2] we decompose the mode shape $\chi(x,y)$ into two parts; the wave part described by a complex wave number α and the shapefunction part ψ to track the nonparallel effect, i.e.,

$$\chi(x,y)=\psi(x,y)e^{i\int_{x_0}^{x}\alpha(\xi)d\xi} \quad (17)$$

in which $\psi=(p,u,v,w,T)$. Here, the integral form is used for the wave part to allow α variation in x and to record the history effect of α. The shape function ψ varies both in x and y. Hence, nonparallel effect is retained through the variation of streamwise wave number and shape function. Substituting Eq.17 into Eq.16, we have

$$A\frac{\partial\psi}{\partial x}+B\frac{\partial\psi}{\partial y}+D\psi=\frac{1}{R_0}\left(\frac{V_{xx}^l}{h_1^2}\frac{\partial^2\psi}{\partial x^2}+\frac{V_{xy}^l}{h_1}\frac{\partial^2\psi}{\partial x\partial y}+V_{yy}^l\frac{\partial^2\psi}{\partial y^2}\right) \quad (18)$$

where matrices A, B, and D are defined by

$$\begin{aligned} A &= \frac{A^l}{h_1} - \frac{2i\alpha V^l_{xx}}{h_1^2 R_0} - \frac{i\beta V^l_{xz}}{h_3 R_0} \\ B &= B^l - \frac{i\alpha V_{xy}}{h_1 R_0} - \frac{i\beta V^l_{xz}}{h_3 R_0} \\ D &= D^l - i\omega\Gamma^l + \frac{i\alpha A^l}{h_1} + \frac{i\beta C^l}{h_3} - (i\frac{d\alpha}{dx} - \alpha^2)\frac{V^2_{xx}}{h_1^2 R_0} \\ &\quad + \frac{\alpha\beta V^l_{xz}}{h_1 h_3 R_0} + \frac{\beta^2 V_{zz}}{h_3^2 R_0}. \end{aligned} \tag{19}$$

The above PDE differs from the LNS equation (Eq.16) only in the terms associated with the wave part α. In fact, a wave part may also be introduced in the LNS solver to increase the numerical accuracy.[15] The harmonic LNS solution procedure may be used to solve Eq.18. However, to improve computational efficiency, a marching procedure is more desirable as long as Eq.18 is parabolic in x. To this end, we neglect the viscous derivatives in x and Eq.18 is reduced to

$$A\frac{\partial v}{\partial x} + B\frac{\partial v}{\partial y} + Dv = \frac{V^l_{yy}}{R_0}\frac{\partial^2 v}{\partial y^2}. \tag{20}$$

Chang et al.[2] pointed out that Eq.20 is only "nearly parabolic" due to the streamwise pressure gradient term $(\partial p/\partial x)$ inherited from the original Navier-Stokes equation 1. Numerical instability similar to that observed in the parabolized Navier-Stokes (PNS) equations[19] will occur if one attempts to solve Eq.20 by using a small enough marching step size. They further suggested that Vigneron's approximation[19] may be used to suppress the numerical instability. Li and Malik[20] use Fourier analysis to prove the existence of numerical instability and quantify the numerical instability bound.

If we retain all nonlinear terms, the governing equations become

$$A_{mn}\frac{\partial v_{mn}}{\partial x} + B_{mn}\frac{\partial v_{mn}}{\partial y} + D_{mn}v_{mn} - \frac{V^l_{yy}}{R_0}\frac{\partial^2 v_{mn}}{\partial y^2} = \frac{F_{mn}}{A_{mn}} \tag{21}$$

where matrices A_{mn}, B_{mn}, and D_{mn} are defined by

$$\begin{aligned} A_{mn} &= \frac{A^l}{h_1} - \frac{2i\alpha_{mn} V^l_{xx}}{h_1^2 R_0} - \frac{in\beta V^l_{xz}}{h_3 R_0} \\ B_{mn} &= B^l - \frac{i\alpha_{mn} V_{xy}}{h_1 R_0} - \frac{in\beta V^l_{xz}}{h_3 R_0} \\ D_{mn} &= D^l - im\omega\Gamma^l + \frac{i\alpha_{mn} A^l}{h_1} + \frac{in\beta C^l}{h_3} \\ &\quad - (i\frac{d\alpha_{mn}}{dx} - \alpha^2_{mn})\frac{V^2_{xx}}{h_1^2 R_0} + \frac{n\alpha\beta V^l_{xz}}{h_1 h_3 R_0} + \frac{n^2\beta^2 V_{zz}}{h_3^2 R_0} \end{aligned} \tag{22}$$

and $A_{mn} = \int_{x_0}^{x} \alpha_{mn} d\xi$. The left-hand side of Eq.21 contains only linear coefficient matrices. All nonlinear terms are included in the forcing function F_{mn}, which is the Fourier component of the total forcing, F^n, defined as

$$\begin{aligned} F^n = &- \Gamma^n\frac{\partial o}{\partial t} - \frac{A^n}{h_1}\frac{\partial o}{\partial x} - B^n\frac{\partial o}{\partial y} - \frac{C^n}{h_3}\frac{\partial o}{\partial z} - D^n o \\ &+ \frac{1}{R_0}(\frac{V^n_{xx}}{h_1^2}\frac{\partial^2 o}{\partial x^2} + \frac{V^n_{xy}}{h_1}\frac{\partial^2 o}{\partial x\partial y} + V^n_{yy}\frac{\partial^2 o}{\partial y^2} \\ &+ \frac{V^n_{xz}}{h_1 h_3}\frac{\partial^2 o}{\partial x\partial z} + \frac{V^n_{yz}}{h_3}\frac{\partial^2 o}{\partial y\partial z} + \frac{V^n_{zz}}{h_3^2}\frac{\partial^2 o}{\partial z^2}) \end{aligned} \tag{23}$$

where the disturbance vector o is defined in physical space (see Eq.9). Nonlinear forcing for each Fourier mode is defined by the following Fourier transform:

$$F^n(x,y,z,t) = \sum_{m=-M}^{M}\sum_{n=-N}^{N} F_{mn}(x,y)e^{i(n\beta z - m\omega t)}. \tag{24}$$

The forcing term F_{mn} for a given Fourier mode (m,n) can be evaluated by collecting all nonlinear terms contributing to it. For instance, the $(0,1)$ mode interacting quadratically with the $(1,0)$ mode would contribute to the $(1,1)$ mode. In LASTRAC, nonlinear forcing terms are evaluated by computing F^n in physical space and then transforming F^n back into the wave number space to obtain F_{mn}.

The governing linear and nonlinear PSE are solved by a fourth-order central difference in the wall-normal direction and a first- or second-order one-sided difference in the marching direction. By invoking the locally parallel assumption, the linear PSE equations may be reduced to the LST eigenvalue problem. LASTRAC is capable of handling LST and linear or nonlinear PSE solutions for a user-supplied mean flow. Details of the discretization scheme and boundary conditions may be found in Ref.[21] The PSE marching solution requires an initial condition, which is discussed in the next section.

Initialization of PSE Marching

The PSE formulation requires an initial condition to start the streamwise marching procedure. A simple way to initiate marching is to use the eigenfunction obtained from the quasi-parallel LST solution. However, because of the neglected nonparallel terms, the marching PSE solution obtained this way would have a "transient" region where the PSE solution attempts to slowly adjust the inconsistent parallel eigenfunctions. This transient effect, more noticeable for supersonic boundary layers, is a result of the difference in governing equations between LST and PSE. To alleviate the transient effect, one can use the multiple-scale method.[22,23] The computed nonparallel eigenvalue and eigenfunction may then be used to initiate the PSE marching procedure.

LASTRAC offers an alternative nonparallel eigensolution (NES) procedure based on the discretized parabolized governing equations. The governing equation is transformed to a general coordinate system by using

$$\xi = \xi(x,y)$$

$$\eta = \eta(x, y).$$

Numerical calculation is then performed in the (ξ, η) plane. Using first-order finite difference in ξ, the governing linear PSE at two consecutive solution locations, i and $i+1$, may be written as

$$\begin{aligned} &\tilde{D}_i \psi_i + \tilde{A}_i(\psi_{i+1} - \psi_i) + \tilde{B}_i \frac{\partial \psi_i}{\partial \eta} = \tilde{V}_{\eta\eta,i} \frac{\partial^2 \psi_i}{\partial \eta^2} \\ &\tilde{D}_{i+1} \psi_{i+1} + \tilde{A}_{i+1}(\psi_{i+1} - \psi_i) + \tilde{B}_{i+1} \frac{\partial \psi_{i+1}}{\partial \eta} \\ &= \tilde{V}_{\eta\eta,i+1} \frac{\partial^2 \psi_{i+1}}{\partial \eta^2}. \end{aligned} \quad (25)$$

For this equation, we assume that the second derivative in ξ is negligible and $\partial\psi/\partial\xi$ is the same for both point i and $i+1$. This assumption is equivalent to taking forward difference for point i and backward difference for point $i+1$. The streamwise wave number α_i and α_{i+1} is related by

$$\alpha_{i+1} = \alpha_i + \frac{d\alpha}{dx}\Delta x \quad (26)$$

in which Δx is the streamwise distance between points i and $i+1$.

If we define the combined shapefunction vector Ψ as

$$\Psi = \begin{pmatrix} \psi_i \\ \psi_{i+1} \end{pmatrix},$$

then Eq.25 may be rewritten as

$$\bar{D}\Psi + \bar{B}\frac{d\Psi}{d\eta} = \bar{V}\frac{d^2\Psi}{d\eta^2} \quad (27)$$

where matrices $\bar{D}$, $\bar{B}$, and $\bar{V}$ are

$$\begin{aligned} \bar{D} &= \begin{pmatrix} \tilde{D}_i - \tilde{A}_i & \tilde{A}_i \\ -\tilde{A}_{i+1} & \tilde{D}_{i+1} - \tilde{A}_{i+1} \end{pmatrix} \\ \bar{B} &= \begin{pmatrix} \tilde{B}_i & 0 \\ 0 & \tilde{B}_{i+1} \end{pmatrix} \\ \bar{V} &= \begin{pmatrix} \tilde{V}_{\eta\eta,i} & 0 \\ 0 & \tilde{V}_{\eta\eta,i+1} \end{pmatrix}. \end{aligned} \quad (28)$$

At the boundaries, homogeneous boundary conditions (e.g. no slip at wall and Dirichlet or nonreflecting conditions at free stream) may be applied for both i and $i+1$ stations. Eq. 27 is a set of homogeneous ordinary differential equations (ODE). After discretization in η, Eq. 27 can be cast into the following nonparallel eigenvalue problem :

$$L_{np}(\Psi) = 0 \quad (29)$$

where $L_{np} = L_{np}(\omega, \alpha, d\alpha/dx, \beta)$. For a given disturbance (ω, β), two eigenvalues α and $d\alpha/dx$ need to be found. Unlike the LST eigenvalue problem, the NES has one more unknown: $d\alpha/dx$. Since the variation of α is generally small, our first approximation is that $d\alpha/dx = 0$. Thus the eigenvalue problem is similar to the LST case, except that the L_{np} operator now contains solutions at two consecutive streamwise stations and requires more time to solve (for both local and global eigenvalue searches). In fact, obtaining the global spectrum with both α and $d\alpha/dx$ as unknowns is nontrivial. In LASTRAC, we assume $d\alpha/dx = 0$ for the solution of the global eigenvalue spectrum.

For the local nonparallel eigenvalue search, as mentioned above, we may assume $\alpha_i = \alpha_{i+1}$. The solution procedure is then similar to the LST case. Alternatively, we may use a local Newton's iteration to solve for α_i and α_{i+1} simultaneously. To this end, we need two target conditions to be iterated upon. If we use u-velocity at the wall, then the wall boundary condition $u_i(0) = u_{i+1}(0) = 0$ is replaced by $p_i(0) = p_{i+1}(0) = 1$. This implies that we will normalize the eigenfunctions such that the pressure eigenfunction is unity at the wall. The relaxed u-velocity condition at the wall becomes the target of the Newton's iterations. In this case, we further assume that the pressure shapefunction at the wall does not vary from station i to $i+1$. For most cases, the wall pressure variation dp/dx is small and the above approximation is valid. If $t_1 = u_i(0)$ and $t_2 = u_{i+1}(0)$, using first-order expansion, we have

$$\begin{aligned} 0 &= t_1 + (\frac{\partial t_1}{\partial \alpha_i})\Delta\alpha_i + (\frac{\partial t_1}{\partial \alpha_{i+1}})\Delta\alpha_{i+1} \\ 0 &= t_2 + (\frac{\partial t_2}{\partial \alpha_i})\Delta\alpha_i + (\frac{\partial t_2}{\partial \alpha_{i+1}})\Delta\alpha_{i+1} \end{aligned} \quad (30)$$

where $\Delta\alpha_i = \alpha_i^{n+1} - \alpha_i^n$ and $\Delta\alpha_{i+1} = \alpha_{i+1}^{n+1} - \alpha_{i+1}^n$ denote the change of eigenvalues from iteration n to iteration $n+1$. Solution of Eq. 30 provides two eigenvalues: α_i and α_{i+1}. The eigenvalue iteration is repeated until $\Delta\alpha_i$ and $\Delta\alpha_{i+1}$ are both smaller than a prescribed tolerance. We have also used the wall temperature instead of the u-velocity as the target condition for Newton's iterations; numerical experiments indicate that both targets worked well. For hypersonic boundary layers, relaxing wall temperature tends to be more robust than wall velocity.

The above non-parallel eigenvalue formulation has several distinct characteristics. First, for every eigensolution, we obtain eigenfunctions at two consecutive locations. Therefore, streamwise derivatives and thus the effective nonparallel growth rates accounting for this streamwise variation may be evaluated. Second, local eigenvalue search using only one alpha ($d\alpha/dx = 0$) is more robust because the global eigenvalue solver is a good approximation to the local solver. However, due to the neglected $d\alpha/dx$, this approximation produces a small but noticeable transient effect (smaller than using the LST solutions) if we use the obtained eigenmode to initiate the PSE marching procedure. Again, this transient effect is more pronounced in supersonic than in low-speed boundary layers for 2-D flows. For crossflow instability, the variation of α near the leading edge is usually large and the one-alpha procedure yields a noticeable transient effect even at low speed.

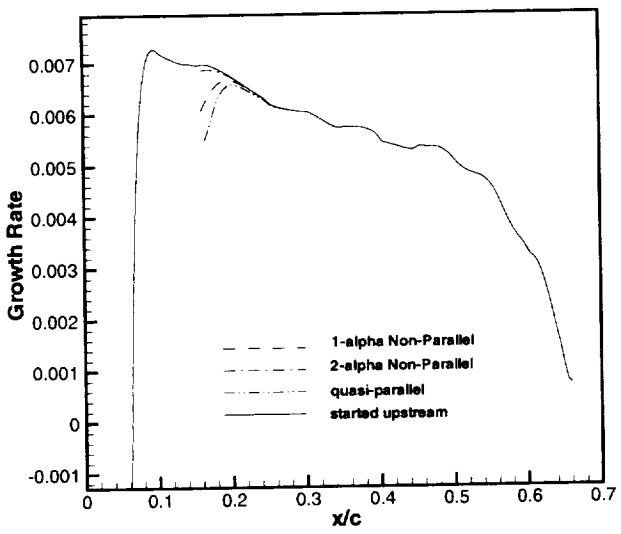

Fig. 3 Linear PSE solution obtained by using three different initial eigenfunctions, compared with the solution initiated far upstream to assess the transient effect

Furthermore, even though this transient effect is noticeable in the disturbance growth rate, it is much less noticeable for the disturbance amplitude which represents the integrated effect of the growth rate. Figure 3 compares linear PSE solutions obtained by the one-alpha, two-alpha, and quasi-parallel LST eigenfunctions. The solution initiated far upstream is also plotted as a baseline solution. Clearly, the two-alpha eigenfunction produces the least transient effect.

On the other hand, the two-alpha iteration procedure is less robust because it requires convergence of two eigenvalues and only first-order Newton's method is employed. Deriving a second-order method is possible but would require introducing more target conditions. The lack of robustness also stems from inconsistency between global and local eigenvalue solvers (noted that in the global solver, we assume $d\alpha/dx = 0$). The initial guess of $d\alpha/dx$ is important for the two-alpha procedure. We have found that for 2-D boundary layers, using the guess from the global solver and imposing $d\alpha/dx = 0$ generally leads to a converged solution. However, for crossflow instability near the leading edge of a swept wing, providing a good guess of $d\alpha/dx$ is crucial to convergence of the eigenvalue search. LASTRAC uses several built-in $d\alpha/dx$ guesses for the two-alpha eigenvalue search. However, in some cases, users need to provide a good guess in order to get a converged eigenvalue. It was also found that the eigensolution obtained with the two-alpha procedure produces minimal transient effects when used to initiate the PSE marching.

As discussed in the previous section, the determination of α is in fact nonunique within the nonparallel framework. The above nonparallel eigenvalue formulation typically generates more discrete eigenmodes than its quasi-parallel LST counterpart. Therefore, selecting eigenmodes of interest from the global eigenvalue spectrum becomes more difficult. Users may need to provide certain additional criteria to filter out spurious modes. Interestingly, one quasi-parallel eigenmode would split into two modes in the corresponding nonparallel global spectrum mainly because we are solving two consecutive eigensolutions simultaneously and we assume that $\alpha_i = \alpha_{i+1}$. We found that with the two-alpha local eigenvalue search, two split modes converge to the same mode. Mathematically, the nonparallel eigenvalue formulation introduces more degrees of freedom in the system and thus allows more discrete eigenmodes (other than the continuous spectrum). The mode closely associated with the unstable mode given by the parallel LST still appears as an eigenmode in most cases. Near the leading edge of the boundary layer, instability wave formation and evolution is governed by the receptivity process; therefore the nonparallel eigenmode may or may not be relevant from the theoretical standpoint. LASTRAC selects the most unstable mode that gives the largest growth rate at the location of interest to initiate the marching procedure. Numerical experiments indicate that the eigenvalue and eigenfunction generated by the NES (both one- and two-alpha approaches) produce a smaller transient effect than those from the quasi-parallel LST solution.

Code Development

The LASTRAC code was developed from scratch. Several guiding principles were set forth in the initial stage of LASTRAC development. They are:

- Object-oriented (OO) design and implementation
- Generic programming using templates
- Optimization to avoid abstraction penalties and ensure efficiency
- Multithread and message passing interface (MPI) based parallelization
- Source code control and some configuration management

The first two items limit the choice of programming language to C++ because it is the only mature language that supports both object-oriented and generic programming. The OO paradigm has been recognized by the software world as a mainstream approach for software development. An OO software system may take longer to develop but it will be much easier to maintain and extend as the project goes along. The concepts of data abstraction, inheritance, and polymorphism are the themes of an object-oriented language. Separation of interface and implementation principle makes software modules more independent of one another.

The common concept for modern software development is to divide the software into a class of similar but not identical objects with a common interface. The clients of these objects only need to know about the interface – not the

implementation details. In this way, new objects may be derived and added to the system without needing to change the common interface or any existing object client's code. Code reuse is thus achieved via reciting common interfaces for various class objects but not through cut-and-paste of existing codes.

The OO design procedure typically employs a formal requirement analysis along with use case studies. The Unified Modeling Language (UML)[24] is a widely used tool for OO analysis and design. Due to the lack of resources, we did not pursue the UML route for analysis and design. Instead, the structure of LASTRAC was laid out based on the numerical formulation and then different design patterns were applied when appropriate. The design patterns used in LASTRAC came mostly from Gamma et al.[25] with some modifications to cope with numerical efficiency. A design pattern is a set of objects and interfaces that occur over and over again in a software system and hence is also a solution to a software problem in a context. Many patterns proposed by Gamma et al. are used in LASTRAC. For example, the Singleton pattern is used for input and control parameters, a Factory Method is used to generate objects on the fly, the Observer pattern is used to let the metric class, coordinate transformation class, and Jacobian matrices class update their contents when the solution marches to the next station. The Template Method and Command patterns are used to implement a multithread class that allows a nonstatic class member function to be called within a C-style thread routine.

Generic programming[26] is a new paradigm that allows a programmer to introduce a parameterized class member or member function in a function or class definition. The introduced parameter is called a template. A routine designed this way allows unrelated classes or algorithms to be plugged in as a template parameter as long as the plugged-in classes fulfill the compilation requirement. For example, one can design a numerical integration class that allows various approximation rules be specified as a template parameter. The C++ programming language includes a powerful library called standard template library (STL) based on the generic programming concept. LASTRAC uses templates extensively in the class design. STL containers and algorithms are used to ensure efficiency and flexibility.

Discussing the details of the LASTRAC code design and structure is beyond the scope of this paper. Here, we only describe important elements of the code structure. Users of LASTRAC need to prepare two files: one contains the mean flow; the other has the input parameters instructing which computation (LST, linear or nonlinear PSE, etc.) needs to be performed. The input parameter file is read by LASTRAC through a parser. The parser takes an input format similar to the namelist format in Fortran but allows C++ style comments. LASTRAC performs a "sanity check" for the input parameter file and flags errors if any user mistake is found. The mean flow reader was designed to be a hierarchy of classes that can be extended for perfect gas/reacting flow, 2-D/3-D through inheritance of the abstract class.

The core part of the code uses the observer pattern (see Gamma et al.[25]) where two subjects, LocalSubject and MarchingSubject, perform a local eigenvalue solution and a marching PSE solution, respectively. The observers are the coordinate transformation, metric and derivatives, and Jacobian classes. These classes update their states when the LocalSubject and MarchingSubject finish their calculations and move on to the next location. The nonlinear marching subject communicates with LocalSubject and MarchingSubject to obtain a local eigenvalue for initiating the marching and to solve for each individual mode during the nonlinear iteration. It has several logistic classes, such as a Fourier container class, to perform fast Fourier transform and to handle Fourier-mode related operations.

The finite difference operation and boundary condition treatment is handled by using a template class and the generic programming paradigm. These generic classes would work for different orders of differentiation and variable types such as real or complex. The left hand side operator of the PSE and eigenvalue solver were cast in an operator form to facilitate future maintenance.

To achieve computational efficiency in the LASTRAC code design, we tried to avoid using many fine-grained objects. The use of templates in generic programming allows substitution of template parameters at compile time; consequently the code can be optimized for run-time performance. In LASTRAC, the template meta-programming technique is used to optimize the matrix multiplication procedure and the block matrix solvers. Extensive use of generic programming and template utilities makes LASTRAC as efficient as an earlier code written in Fortran 77.

Parallelization for the nonlinear PSE option in LASTRAC is implemented by using the multithread technique in conjunction with the more traditional MPI approach. Posix thread is used in LASTRAC to guarantee portability. Multithread and MPI options are only implemented for nonlinear PSE calculations. Linear options, including LST and linear PSE, can only be run as single-thread applications. Since linear calculations are mode independent, users can launch many LASTRAC runs concurrently on a multiprocessor or clustered environment.

For nonlinear PSE calculations, each Fourier mode is solved by a thread or a process under MPI. However, the nonlinear forcing terms have to be computed collectively. Parallelization of nonlinear forcing is only done through computing terms in physical space simultaneously. Each MPI process may spawn multiple threads. For a multiprocessor node in a cluster, this combined thread and MPI approach makes LASTRAC run more efficiently.

Source code control and configuration management is performed through the public domain software CVS. Unit testing was accomplished for major modules during the initial development stage. Due to lack of resources, we do not follow unit and integration testing procedures rigorously. A semi-automated integration testing procedure is also im-

plemented.

LASTRAC code has been ported to all major Unix platforms. In the release, we include executables for Linux Intel, SUN Solaris, and SGI. We are planning to port the code for Linux Alpha and Windows in the near future.

Code Validation and Test Cases

The LASTRAC code was validated by comparing its results with those obtained in the literature and by other publicly available codes. The first case used for validation was the quasi-parallel LST results published by Malik.[27] The test cases range from low-speed (incompressible) to hypersonic conditions. Linear and nonlinear PSE results were compared with those given in Chang et al.[2,28,29] For swept wing boundary layers, the Arizona State University test configuration[30] was used for validation, and results were compared with Malik et al.[3] For all these validation cases, the results compared very well with existing solutions. To demonstrate the use of LASTRAC, we discuss several test cases in details below.

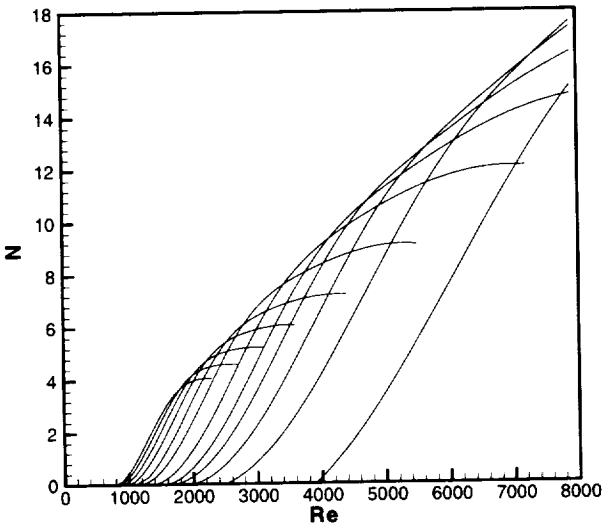

Fig. 4 Maximized N-factor vs. Reynolds number for f from 2 kHz to 45 kHz for a Mach 2 flat plate boundary layer

Mach 2 Flat Plate

The first case is a Mach 2 flow over a flat plate. LASTRAC reads the mean flow and prints out a summary as follows:

```
 /*  Mean Flow Parameters Reading in *\

Title                    : Mach 2 Flat Plate
GasModel                 : Perfect gas model
Reference Mach Number    : 1.99986
Prandtl Number           : 0.7
No. of Stations          : 401
X Coordinate Range(m)    : 0.000 -   1.951
Re Range                 : 0.100 -   8000.000
```

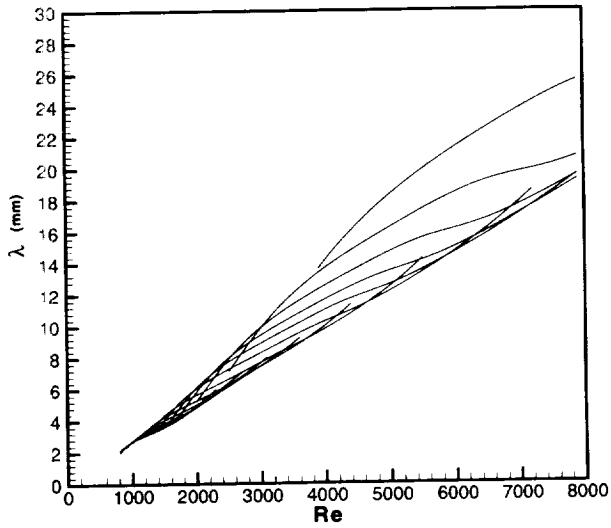

Fig. 5 Maximized spanwise wavelength vs. Reynolds number for f from 2 kHz to 45 kHz for a Mach 2 flat plate boundary layer

```
B.L. Length Scale(m)   : 3.0E-09 - 2.4E-04
U_inf Velocity (m/s)   : 590.065 - 590.065
T_inf Temperature (K)  : 216.667 - 216.667

\*  ..............................  */
% disturbance reference frequency in Hz %
   ranging from 153150 to 88310.4 for 1/d = 2
     or  from 25524.9 to 14718.4 for 1/d = 12
```

In addition to mean flow characteristic, a disturbance frequency range for unstable waves is also suggested. Based on this frequency range, an input file containing the following may be used to find maximized growth rates with respect to the spanwise wavenumber β:

```
//
//  Mach 2 flat plate
//
num_normal_pts        =101

mflow_filename = "../meanflow/mflow.m2fp"

marching_method_2d    = along_re
init_re =  500,  final_re = 7900,
step_re = 100,

solution_type       = local_eig_solution

lod_max = 25

freq_unit           =  in_hertz_freq
beta_unit           =  wave_angle_beta

freq = 2e3, 4e3, 6e3, 8e3, 10e3, 12e3, 15e3,
20e3, 25e3, 30e3, 35e3, 40e3, 45e3,
```

```
beta = 13*60,

qp_approx          = true
```

Figure 4 shows the resulting N-factor versus Reynolds number for various disturbance frequencies. The corresponding spanwise wavelength in millimeters is shown in Fig. 5. It indicates that the unstable spanwise wavelength is around 4 to 20 mm. The N-factor shown in Fig. 4 may be used for transition correlation or prediction directly. However, it has been found that N-factor correlation based on individual modes rather than maximized modes represents the physics better and thus gives better transition correlation with respect to experimental data. Given the unstable frequency and spanwise wavelength range, further calculations such as LST or linear PSE may be done for individual modes. Or if the initial disturbance amplitudes are known from receptivity calculations or experimental data, nonlinear PSE may be launched for a number of unstable waves to track transition onset.

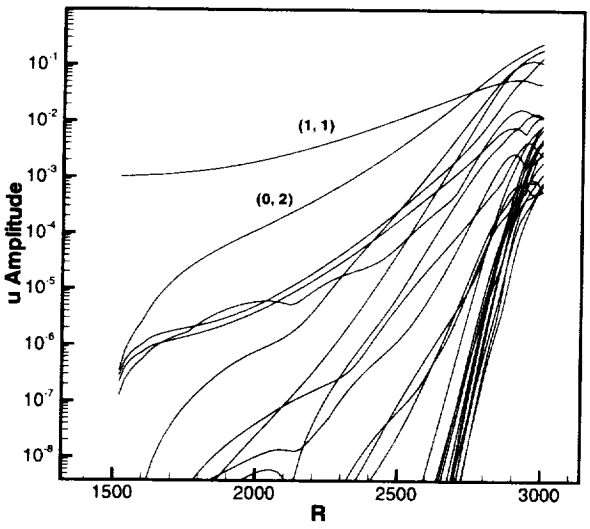

Fig. 6 Evolution of disturbance modal amplitudes for a Mach 2 flat plate undergoing an oblique-mode breakdown

As shown in Fig. 4, a disturbance with a frequency of 12 kHz reaches an N-factor of 10 first. The associated maximized spanwise wavelength is about 8 mm. We initiate a nonlinear PSE calculation at $R = 1500$ with a pair of oblique modes with $f = 12$ kHZ and $\lambda_z = 8$ mm (Fourier mode (1, 1) and (1, -1)). The initial amplitude is 0.1% for both modes. The resulting streamwise velocity amplitude versus Reynolds number is shown in Fig.6 for various Fourier modes. Mutual interaction of the oblique pair gives rise to the excitation and growth of the (0, 2) mode. Nonlinear interaction of this triad then cascades energy into higher harmonics and eventually causes transition. The skin friction is plotted in Fig.7. The rapid rise near the end illustrates that the flow is transitional. More details concerning this oblique-mode breakdown may be found in

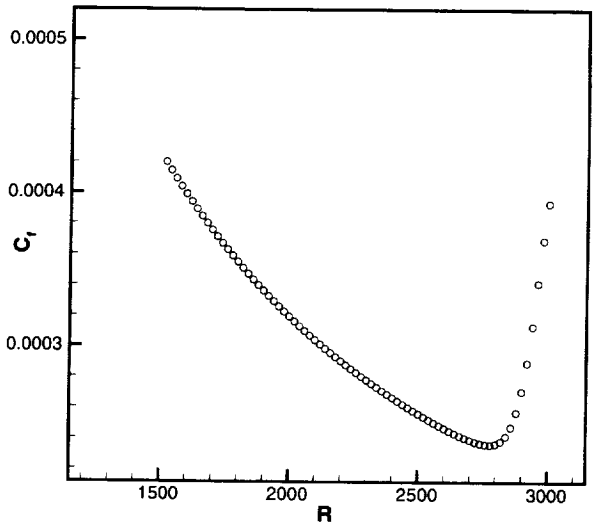

Fig. 7 Skin friction coefficient vs. Reynolds number for a Mach 2 flat plate boundary layer undergoing an oblique-mode breakdown

Chang & Malik.[6]

This example shows a typical work flow how LASTRAC may be used for stability calculations and transition predictions. For a given mean flow, the unstable frequency and spanwise wavelength range may be found with minimum effort and without too much prior knowledge of the flow. After identifying this range, N-factor correlations or predictions using either LST or linear PSE may be performed. For a given initial amplitude, nonlinear PSE may also be used to track nonlinear development of the instability wave all the way until skin friction rise.

Mach 6 Flared Cone

Another test case is a Mach 6 flared cone for which experimental measurements have been conducted in the Langley Mach 6 20-in tunnel.[31] The experimental model is a 5° straight cone for the first 10 in. followed by a flared section. At a free-stream Mach number of 6, the boundary layer edge Mach number inside the shock is about 5.4. The dominant instability mode is hence second mode. The second-mode wave is most unstable when it is two-dimensional or axisymmetric. All second-mode calculations presented here were done for axisymmetric waves. The asymmetric first-mode waves were computed by using different azimuthal wave numbers, n, defined as the number of waves along the azimuthal direction.

Figure 8 shows quasi-parallel LST N-factors of various disturbance frequencies (ranging from 20 to 340 kHz) versus the streamwise distance x for a unit Reynolds number of 2.89×10^6 /ft. This case corresponds to the earlier Mach 6 quiet wind-tunnel measurements with a unit Reynolds number of 2.81×10^6 /ft. The N-factor value at the transition onset is merely 3.8 under the conventional tunnel conditions, as compared to a value of about 7.8 under the

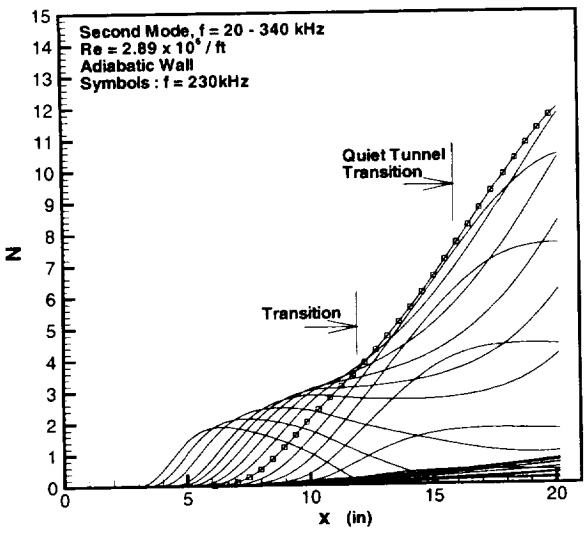

Fig. 8 Second-mode N-factors of various disturbance frequencies for the Mach 6 flared cone with a unit Reynolds number of 2.89×10^6 /ft at adiabatic wall conditions

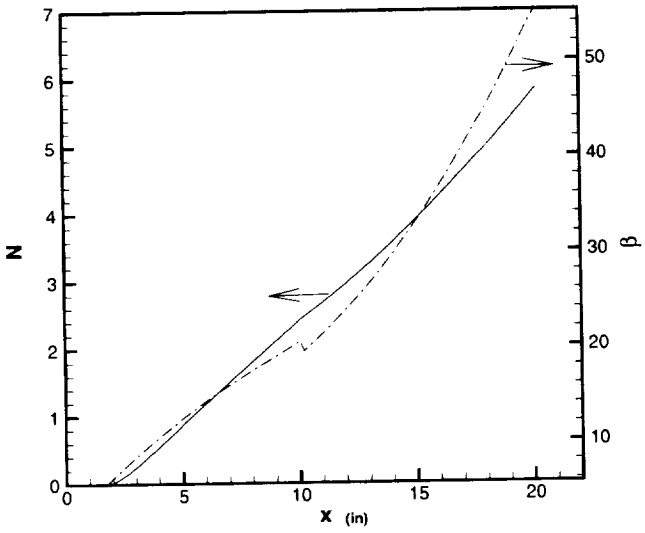

Fig. 9 Optimized first mode N-factor vs. Reynolds number for the Mach 6 flared cone, f = 60 kHz, also showing corresponding integer azimuthal wave number on the plot

quiet tunnel conditions.

Figure 9 depicts the N-factor and corresponding maximized integer azimuthal wave number for a typical first-mode frequency of 60 kHz. The kink on the wave number curve near $x = 10$ in. is due to the curvature discontinuity in the presence of the flare. The results show that the first mode is most unstable for n ranging from 10 to 50. Using this information, first-mode N-factors are calculated for a disturbance frequency ranging from 40 to 100 kHz and an azimuthal wave number from $n = 3$ to $n = 30$ and the results are shown in Fig. 10. The most amplified azimuthal

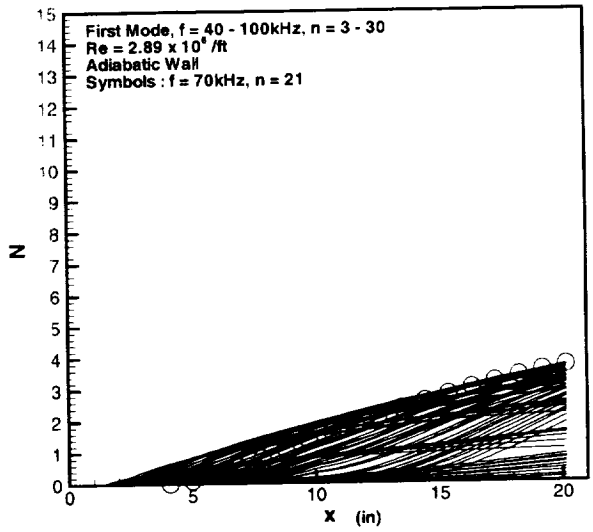

Fig. 10 First-mode N-factors of various disturbance frequencies and azimuthal wave numbers for a unit Reynolds number of 2.89×10^6 /ft at an adiabatic wall condition

wave number was found to be around 20 for most cases. The first-mode N-value at transition onset measured in the conventional (non-quiet) tunnel is only about 2 to 3 which is comparable to the second mode.

Jet and Shear Layer

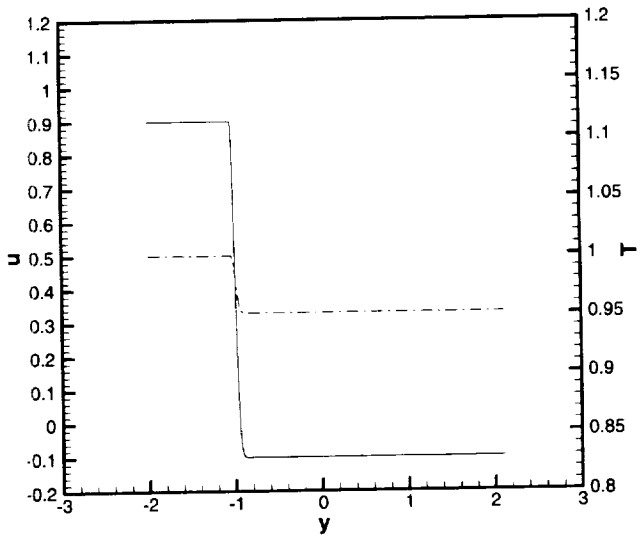

Fig. 11 Velocity and temperature profiles for a compressible shear layer

LASTRAC may also be used for jet and shear layer instability calculations. A shear layer with hyperbolic tangent velocity and temperature profiles, as shown in Fig.11, is used as a test case. The computed velocity and temperature eigenfunctions are shown in Fig.12. LASTRAC can be used to compute axisymmetric jets or vortex flows. The

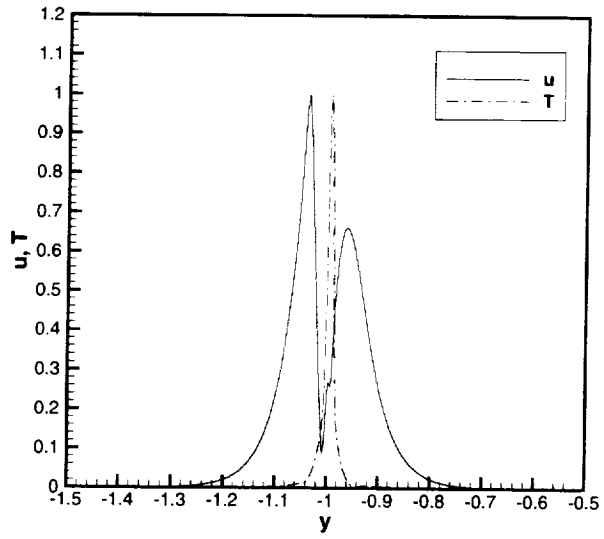

Fig. 12 Velocity and temperature eigenfunction of an unstable mode for a compressible shear layer at f = 8000 Hz

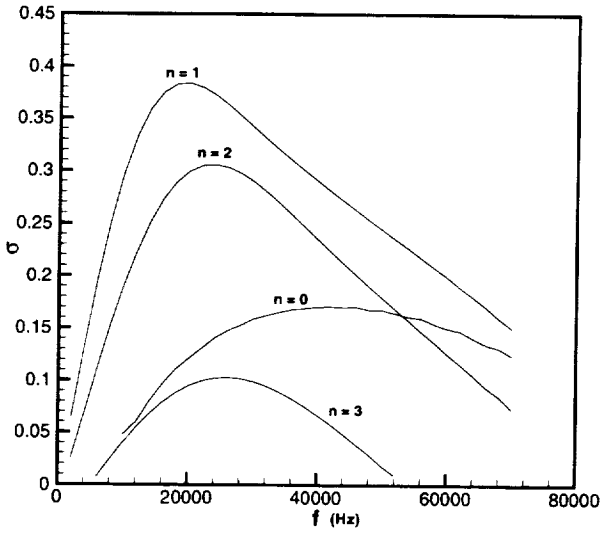

Fig. 13 Growth rates vs. disturbance frequency for the Mach 2.5 jet at x = 0.02 m for different azimuthal wave numbers

test case is a Mach 2.5 jet. The computed growth rates versus disturbance frequencies are show in Fig.13 for various azimuthal wave numbers ranging from 0 (axisymmetric mode) to 3.

Thermal Control of Supersonic Crossflow Instability

Recently, the concept of supersonic thermal laminar flow control has been proposed as an alternative to existing technologies based on either natural laminar flow design or suction. Thermal control does not suffer from major drawbacks of shaping or suction and has the potential to offer an effective control with lower system penalties and fewer restrictions on airframe design. This case is intended to study the effect of cooling on supersonic swept wing boundary layers.

Viscosity is a strong function of temperature; it follows that wall cooling directly affects the stability characteristics of viscous-mode instability waves. For gases, heating destabilizes while cooling stabilizes. Conversely, heating stabilizes a water boundary layer. Examples of viscous modes include the incompressible Tollmien-Schlicting (TS) wave and the first-mode wave in compressible boundary layers which is in fact a mixture of viscous and inviscid mode.[32] For inviscid modes, the effect of wall cooling is more intricate. The addition of a new generalized inflection point due to wall cooling directly alters the stability characteristics. Mack[32] performed both inviscid and viscous stability calculations on first- and second-mode waves and concluded that in general, cooling stabilizes first-mode disturbances and it destabilizes higher modes such as a second-mode disturbance.

For swept wing boundary layers, crossflow instability is the dominant instability mechanism. This inviscid instability arises because of the presence of an inflection point in the crossflow profile in the direction perpendicular to the free-stream direction. As a result, for incompressible swept wing boundary layers, wall cooling has little effect on its growth. On the other hand, wall cooling may still affect supersonic crossflow instability in a significant way because of the presence of an additional generalized inflection point in the mean flow profiles.

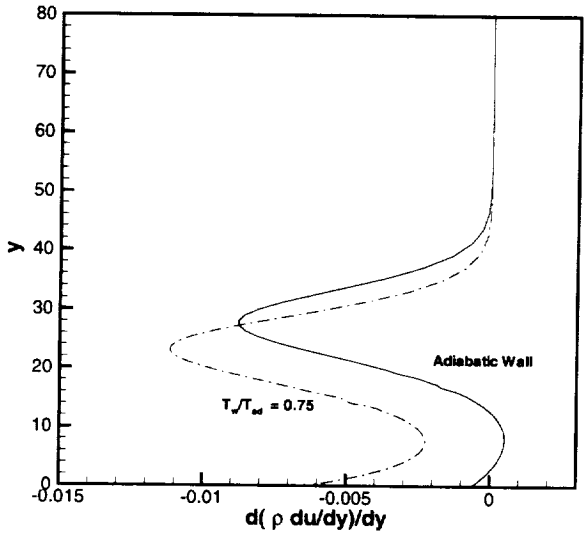

Fig. 14 Generalized inflection point for the streamwise velocity component for an adiabatic and cooled wall, Mach 2 infinite swept wing boundary layer

We use a Mach 2 flow over a 70° infinite swept wing boundary layer as the test example for thermal control. Before showing the stability results, we will examine the effect of cooling on the mean flow profiles first. The necessary condition for inviscid instability in compressible boundary layers is the presence of a generalized inflection

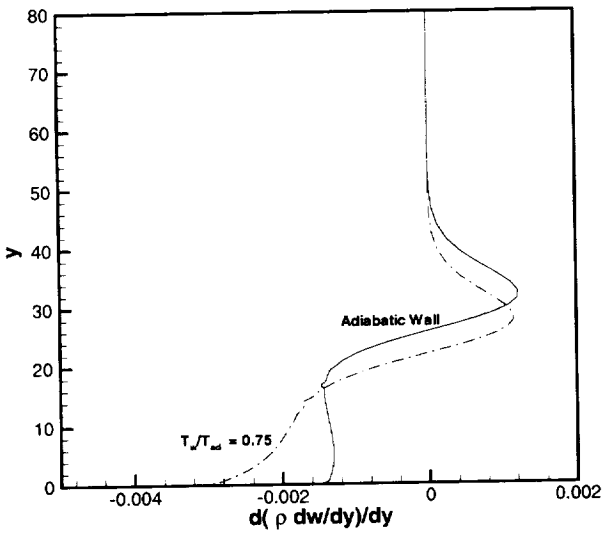

Fig. 15 Generalized inflection point for the crossflow velocity component for an adiabatic and cooled wall, Mach 2 infinite swept wing boundary layer

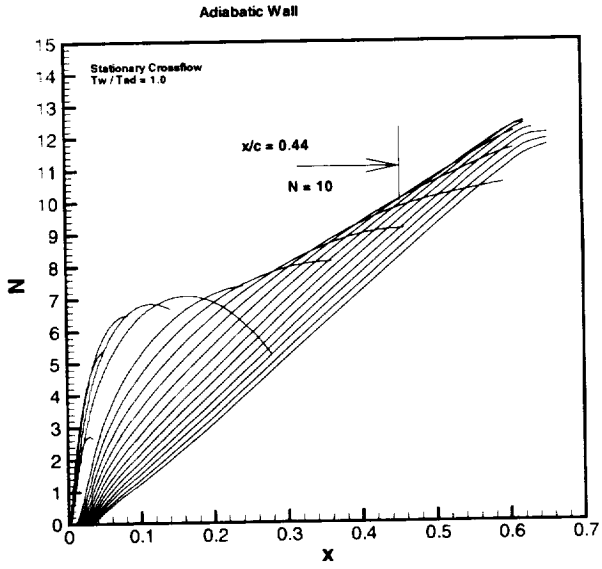

Fig. 16 N-factor vs. x/c for stationary crossflow for a Mach 2, 70° swept wing with an adiabatic wall condition

point characterized by

$$\frac{d}{dy}(\rho\frac{du}{dy}) = 0.$$

The generalized inflection quantity $\frac{d}{dy}(\rho\frac{du}{dy})$ for the above boundary layer with an adiabatic and cooled wall ($T_w/T_{adw} = 0.75$) condition is shown in Fig.14 and 15 for the streamwise and crossflow profiles, respectively. As can be seen in Fig. 15, cooling simply moves the inflection point of the crossflow velocity profile toward the wall but does not remove it. In contrast (Fig. 14), two streamwise inflection points in the adiabatic wall case disappear as we apply cooling. It is interesting to note that the inflection points in the streamwise velocity profile are not present in the incompressible case.

Our linear stability calculations show that similar to first-mode waves, cooling stabilizes both stationary and traveling low supersonic crossflow instability. The main difference is that cooling is much more effective for first-mode waves that appear in 2-D boundary layers. For a Mach 2 flat plate, $T_w/T_{adw} = 0.95$ is sufficient to reduce the N-factor significantly. However, in the present Mach 2 swept wing, a cooling of $T_w/T_{adw} = 0.75$ or lower is necessary to have a significant effect. Nevertheless, cooling still is an effective means to control supersonic crossflow instability. Figures 16 and 17 show the N-factor versus x/c for stationary crossflow instability with an adiabatic and partially cooled (with $T_w/T_{adw} = 0.75$ for $x/c < 0.1$) wall, respectively. If we take $N = 10$ as the transition location, this partially cooled wall brings transition location from $x/c = 0.52$ to $x/c = 0.44$, a 15% reduction. The above results indicate that for supersonic crossflow instability, thermal control is a viable alternative to existing technologies. More parametric studies are necessary to draw a more concrete conclusion.

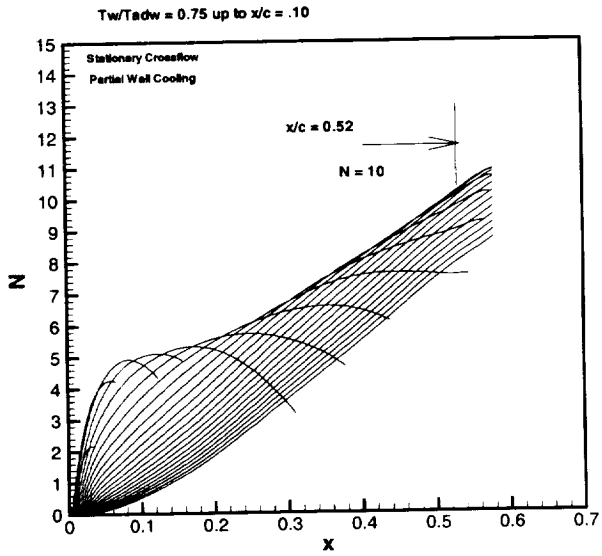

Fig. 17 N-factor vs. x/c for stationary crossflow for a Mach 2, 70° swept wing with $T_w/T_{adw} = 0.75$ for $x/c < 0.1$

Distributed Roughness Control

This test case is concerned with the distributed roughness control proposed by Saric.[33] The incompressible Arizona State University swept wing[30] boundary layer is first analyzed by using LST. Unstable stationary crossflow disturbances are identified by using the eigenvalue solution procedure. The unstable modes have a spanwise wavelength from 3 to 30 mm. Figure 18 shows some of the representative modes. In a distributed roughness control, we manually excite an early growing mode such as the 8-mm mode in this case using a distributed roughness near the

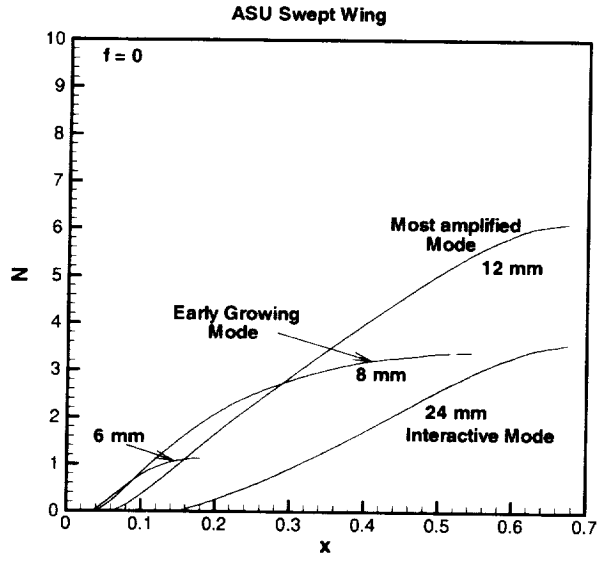

Fig. 18 Important stationary crossflow modes for the incompressible Arizona State University swept wing experiment

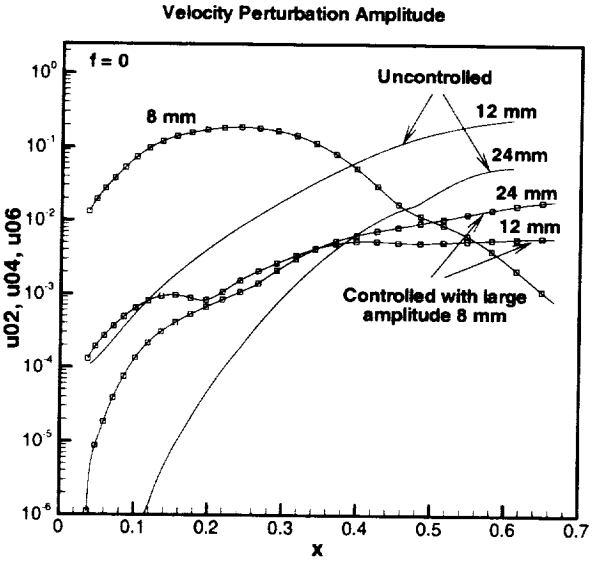

Fig. 19 Nonlinear evolution of the 12-mm and 24-mm modes with and without the presence of the controlled 8-mm mode for the incompressible ASU swept wing experiment

leading edge. This early growing mode will grow to a large amplitude near the leading edge and its growth modifies the mean flow to an extent that the normal growth of the most amplified mode with a wavelength of 12 mm would be suppressed. In the mean time, the 8-mm mode rapidly enters the decaying stage downstream because of the nature of the short wavelength modes. Eventually, all unstable modes involved die out and laminar flow is maintained before the end of the chord. Nonlinear PSE was run for two cases. The uncontrolled case was run with an initial amplitude of about 0.01% for the 12-mm mode. For the controlled case, we introduce an additional 8-mm mode with an initial amplitude of about 1%. As shown in Fig.19, the uncontrolled case reaches an amplitude of about 15% near the end of simulation. On the other hand, the controlled case has a final amplitude less than 2% for both 8-mm and 12-mm modes (as well as its harmonic 24-mm mode). Transition in this configuration is related to secondary instability of the highly nonlinear stationary crossflow modes. Smaller amplitude in the controlled case would prevent secondary instability and thus transition from happening. These cases were run with 24 Fourier modes ($M = 0, N = 24$).

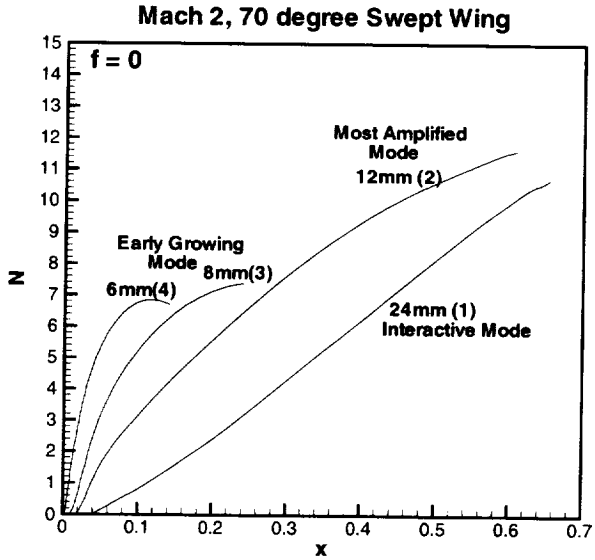

Fig. 20 Important stationary crossflow modes for the Mach 2, 70° swept wing boundary layer

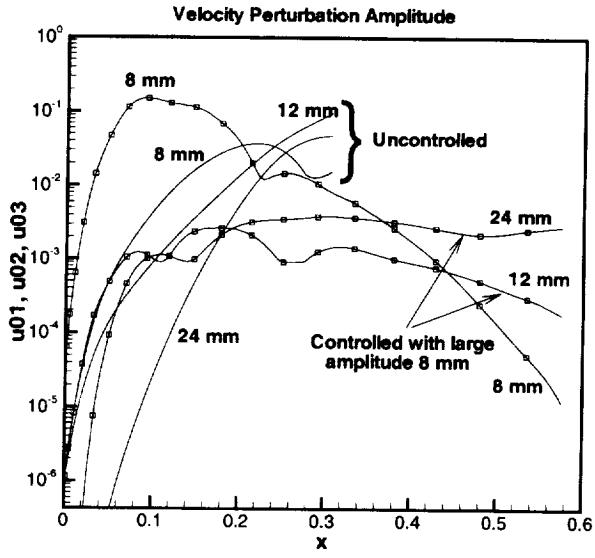

Fig. 21 Nonlinear evolution of the 12-mm and 24-mm modes with and without the presence of the controlled 8-mm mode for the Mach 2, 70° swept wing boundary layer

To investigate whether a distributed roughness control would work for supersonic boundary layers, we study the

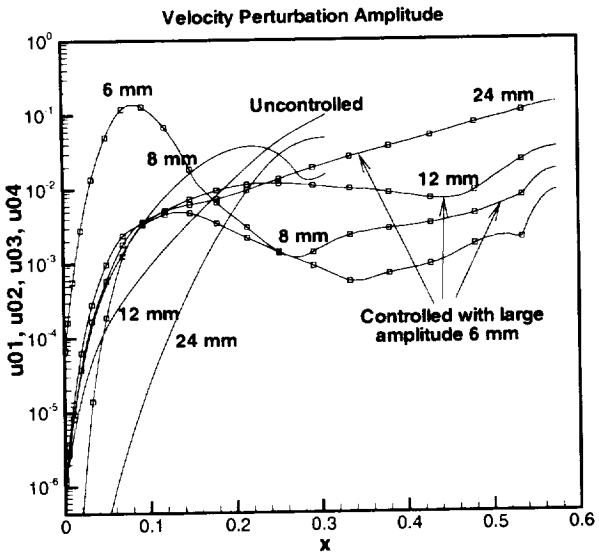

Fig. 22 Nonlinear evolution of the 12-mm and 24-mm modes with and without the presence of the controlled 6-mm mode for the Mach 2, 70° swept wing boundary layer

Mach 2, 70° swept wing configuration used previously for thermal control again. Figure 20 shows the N-factor for the most amplified along with other representative modes. The most amplified wave is at $\lambda_z = 12$ mm and both 6-mm and 8-mm waves appear to be a good candidate for the control. Note that the 24-mm mode also has a large N-factor at the end. For the uncontrolled calculation, we excite both the 12-mm and 8-mm modes with an initial amplitude of $1.e-6$. The fundamental spanwise wavelength is 24 mm and 32 modes ($N = 32$) are kept in the Fourier series.

The first control is to utilize the 8-mm mode. We increase the initial amplitude of the 8-mm mode an order of magnitude larger to $5.e-5$. The results are shown in Fig. 21. For the uncontrolled case, the 8-mm mode grew early on but it was overtaken by the 12-mm mode at around $x/c = 0.22$, the harmonic 24-mm mode also grew to a quite large amplitude near the end of the calculation. For the controlled case, the 8-mm mode was dominating early on then started to decay not too far downstream. As a result, both 12-mm and 24-mm modes were suppressed. The final amplitude for the controlled case is at least one and half orders of magnitude smaller than the uncontrolled case.

For the second control, we introduce the 6-mm mode as the (0, 4) mode in the nonlinear calculation. The initial amplitudes of the 12-mm and 8-mm modes are set to $1.e-6$ and the control mode 6-mm has an amplitude of $5.e-5$. Figure 22 shows the results. The 6-mm control mode grew early on and was dominating for $x/c < 0.18$. It then decayed rapidly. Similar to the 8-mm control case discussed previously, the growth of 12-mm and 8-mm modes was suppressed by the presence of the large amplitude 6-mm mode. However, the rapid growth of the $24mm$ mode at the end appears to be unavoidable. This 24-mm mode excited by nonlinear interaction of the 6-mm and 8-mm ((0, 4) and (0, 3) modes) as well as 8-mm and 12-mm ((0, 3) and (0, 2) modes) grew very rapidly from the beginning. Furthermore, for $x/c > 0.25$ where other modes are decaying, this 24-mm mode begins to dominate due to its large linear growth rate (see Fig.20). Therefore, the 6-mm control is not as effective as the 8-mm one as shown in Fig. 21. Depending on the initial amplitude, in this case, the introduction of the 6-mm mode may or may not achieve laminar flow control because of the presence of the very unstable longer wavelength mode.

This example shows that the selection of the control mode is crucial to the success of distributed roughness control. For the latter supersonic swept wing case, linearly, the unstable stationary crossflow modes cover a large spanwise wave number range, which is a characteristic of large Reynolds number configurations. As a result, nonlinear interaction of the control mode and the most amplified mode may give rise to a longer wavelength mode that would eventually dominate downstream. When this happens, using distributed roughness with a single spanwise wavelength would fail according to our nonlinear PSE results shown here. However, introducing multiple-scale distributed roughness may still work. Further parametric study is necessary to draw a more concrete conclusion. The results presented here also demonstrate the importance of parametric study using nonlinear PSE for a nonlinear control concept such as the distributed roughness control. LASTRAC provides one such tool for future design studies.

Incompressible Subharmonic Breakdown

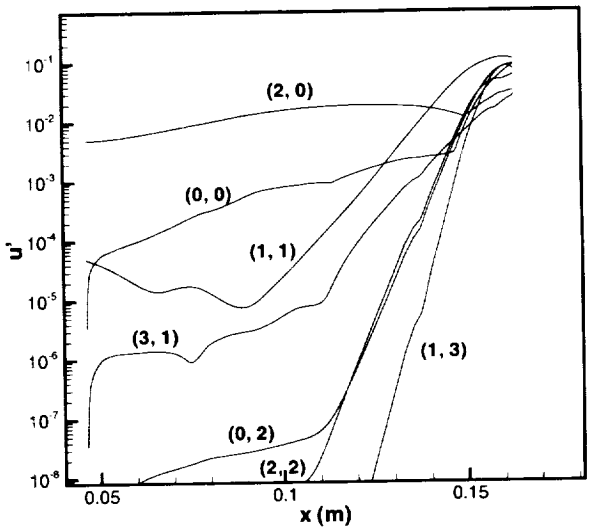

Fig. 23 Nonlinear evolution of selected Fourier modes for subharmonic breakdown to turbulence in a Blasius boundary layer

The last test case is the well-known incompressible subharmonic breakdown phenomena. The fundamental mode is a 2-D mode (mode (2, 0)) with a frequency of $F =$

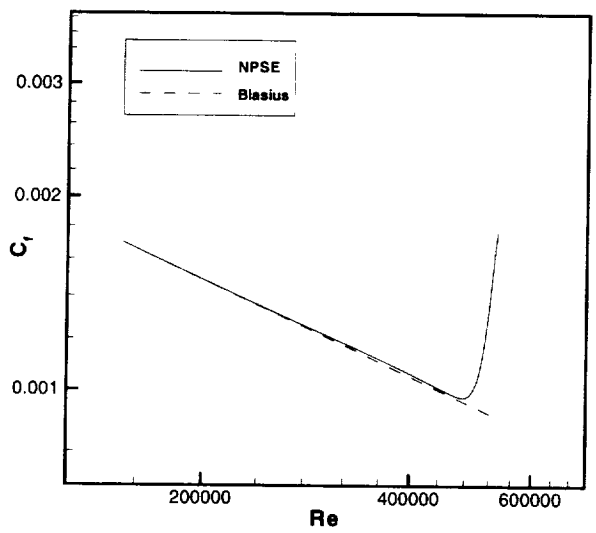

Fig. 24 Skin friction coefficient versus Reynolds number for the subharmonic breakdown in a Blasius boundary layer

1.24×10^{-4}. The subharmonic mode (mode $(1,1)$) has a nondimensional (normalized with the boundary layer length scale) spanwise wavenumber of about $\beta = 0.14$. Initial amplitudes are about 0.5% and 0.005% for the fundamental and subharmonic modes, respectively. We use six Fourier modes in both temporal and spanwise directions ($M = 6, N = 6$). Figure 23 shows the u velocity amplitude evolution for the fundamental, subharmonic and some representative modes. Secondary instability takes place early on; and nonlinear interaction results in excitation of many harmonics. Near the end of the simulation, the fundamental mode is forced to grow again (back reaction) as the subharmonic mode saturates. The skin friction for the perturbed nonlinear PSE solution is plotted against the Blasius (laminar) solution in Fig. 24. A rapid rise of skin friction is evident.

Summary

Predicting transition onset remains a daunting task even with the state-of-the-art computing facilities. At the lowest fidelity, transition may be predicted by using a prescribed N-factor and a simple linear stability or parabolized stability theory. Depending on the accuracy requirement, the N-value may come from empirical correlations with existing wind tunnel or flight experiments, or from a commonly used value such as 10. The major problem of this approach lies in the N-value itself. According to past experiences, the transition N-value may vary from as small as 2 or 3 for a noisy facility to as high as 15 or 20 in flight. Thus, for a new configuration, determining the N value is itself a difficult task. Despite this uncertainty, N-factor correlation remains the most viable method for transition prediction due to its simplicity. LASTRAC provide both LST- and PSE-based N-factor correlation capability.

For a given mean flow, a possible unstable frequency range is suggested by LASTRAC and by using the maximizing N-factor option, users may obtain an unstable parameter range of disturbance frequency and spanwise wavelength with minimum effort and little prior knowledge of the mean flow under consideration. Further linear calculations using either quasi-parallel LST or nonparallel PSE may be launched to obtain an envelop of N-factors formed by a broad range of unstable modes. The N-factor envelope then can be used for transition correlations or predictions.

LASTRAC also provides the capability to compute disturbance evolution based on an absolute amplitude. Nonlinear PSE calculations may be performed for a number of unstable modes with a finite amplitude. We show several test cases in which the boundary layer is perturbed with a given amplitude and transition is captured by using the nonlinear PSE option. Coupled with the receptivity model which will be incorporated in the near future, LASTRAC offers a transition prediction tool that may be used to compute transition onset without any modeling or N-factor assumptions.

It is also demonstrated that LASTRAC may be used for parametric studies of several supersonic laminar flow control concepts. We presented two such techniques, thermal and distributed roughness control. The test cases shown in this paper cover a broad range of flow configurations. In addition to the traditional N-factor method, LASTRAC offers a comprehensive set of options based on the state-of-the-art numerical methods that may be used for the stability calculations and transition predictions in an integrated fashion.

Acknowledgment

The author would like to thank Dr. Meelan Choudhari for his great help throughout the course of LASTRAC development.

References

[1] Kroo, I., Tracy, R., Chase, J., and Sturdza, P., "Natural Laminar Flow for Quiet and Efficient Supersonic Aircraft," AIAA Paper-2002-0146, 2002.

[2] Chang, C.-L., Malik, M. R., Erlebacher, G., and Hussaini, M. Y., "Compressible Stability of Growing Boundary Layers Using Parabolized Stability Equations," AIAA Paper-1991-1636, 1991.

[3] Malik, M., Li, F., Choudhari, M., and Chang, C.-L., "Secondary Instability of Crossflow Vortices and Swept-wing Boundary-Layer Transition," *J. Fluid Mech.*, Vol. 399, 1999, pp. 85–115.

[4] Saric, W. S., Carrillo, R. B., and Reibert, M. S., "Leading-Edge Roughness as a Transition Control Mechanism," AIAA Paper, 98-0781, 1998.

[5] Chang, C.-L., "Thermal Effect on Crossflow Instability in Supersonic Boundary Layers," 14th US National Congress of Theoretical and Applied Mechanics, 2002.

[6] Chang, C.-L. and Malik, M. R., "Oblique-Mode Breakdown and Secondary Instability in Supersonic Boundary Layers," *J. Fluid Mech.*, Vol. 273, 1994, pp. 323–359.

[7] Stetson, K. F., Thompson, E. R., Donaldson, J. C., and Siler, L. G., "Laminar Boundary Layer Stability Experiments on a Cone at Mach 8 Part I: Sharp Cone," AIAA Paper-83-1761, 1983.

[8] Lachowicz, J. T., Chokani, N., and Wilkinson, S. P., "Boundary-Layer Stability Measurements in a Hypersonic Quiet Tunnel," *AIAA J.*, Vol. 34, 1996, pp. 2496–2500.

[9]Horvath, T. J., Berry, S. A., Hollis, B. R., Chang, C.-L., and Singer, B. A., "Boundary Layer Transition On Slender Cones In Conventional and Low Disturbance Mach 6 Wind Tunnels," AIAA Paper-2002-2743, 2002.

[10]Fedorov, A., "Receptivity of High Speed Boundary Layer to Acoustic Disturbances," AIAA Paper-2002-2846, 2002.

[11]Zhong, X. and Ma, Y., "Receptivity and Linear Stability of Stetson's Mach 8 Blunt Cone Stability Experiments," AIAA Paper-2002-2849, 2002.

[12]Fedorov, A. and Tumin, A., "Evolution of Disturbances in Entropy Layer on a Blunted Plate in Supersonic Flow," AIAA Paper-2002-2847, 2002.

[13]Saric, W. S. and Reed, H. L., "Supersonic Laminar Flow Control on Swept Wings Using Distributed Roughness," AIAA Paper-2002-0147, 2002.

[14]Streett, C. L., "Direct Harmonic Navier-Stokes Methods for Efficient Simulation of Weakly-Nonlinear Wave Packets," AIAA Paper-1998-0784, 1998.

[15]Yan, G., Malik, M. R., and Chang, C.-L., "A Solution Adaptive Approach for Computation of Linear Waves," AIAA Paper-1997-2072, 1997.

[16]Rubinstein, R. and Choudhari, M., "Statistical Prediction of Laminar-Turbulent Transition," ICASE Report, 2000-50, 2000.

[17]Choudhari, M., Chang, C.-L., Streett, C. L., and Balakumar, P., "Integrated Transition Prediction: A Case Study in Supersonic Laminar Flow Control," AIAA Paper-2003-0973, 2003.

[18]Herbert, T., "Boundary-Layer Transition – Analysis and Prediction Revised," AIAA Paper-2002-0147, 2002.

[19]Vigneron, Y. C., Rakich, J. V., and Tannehill, J. C., "Calculation of Supersonic Viscous Flow Over Delta Wings with Sharp Supersonic Leading Edges," AIAA Paper, 78-1337, 1978.

[20]Li, F. and Malik, M. R., "On the Nature of PSE Approximation," *Theoret. and Comput. Fluid Dynamics*, Vol. 8, 1996, pp. 253–273.

[21]Chang, C.-L., "The Langley Stability and Transition Analysis Codes (LASTRAC) User Manual," NASA TM, in preparation, 2002.

[22]El-Hady, N. M., "Non-Parallel Instability of Supersonic and Hypersonic Boundary Layers," AIAA Paper-1991-0324, 1991.

[23]Saric, W. S. and Nayfeh, A. H., "Non-Parallel Stability of Boundary-Layer Flows," *Phys. Fluids*, Vol. 18, 1975.

[24]Rumbaugh, J., Jacobson, I., and Booch, G., *The Unified Modeling Language Reference Manual*, Addison Wesley, 1999.

[25]Gamma, E., Helm, R., Johnson, R., and Vlissides, J., *Design Patterns*, Addison Wesley, 1995.

[26]Stepanov, A. and Lee, M., "The Standard Template Library," Technical Report HPL-95-11 (R.1), Hewlett-Packard Laboratories, 1995.

[27]Malik, M. R., "Numerical Methods for Hypersonic Boundary Layer Stability," *J. Comput. Physics*, 1989, pp. 376–413.

[28]Chang, C.-L. and Malik, M. R., "Non-Parallel Stability of Compressible Boundary Layers," AIAA Paper-1993-2912, 1993.

[29]Chang, C.-L., Malik, M. R., and Vinh, H., "Linear and Nonlinear Stability of Compressible Swept-Wing Boundary Layers," AIAA Paper-1995-2278, 1995.

[30]Reibert, M., Saric, W. S., Carrillo, R. B. J., and Chapman, K. L., "Experiments in Nonlinear Saturation of Stationary Crossflow Vortices in a Swept-Wing Boundary Layer," AIAA Paper, 96-0184, 1996.

[31]Hovath, T. J., Berry, S. A., Hollis, B. R., Chang, C.-L., and Singer, B. A., "Boundary Layer Transition on Slender Cones in a Conventional and a Low Disturbance Mach 6 Wind Tunnel," AIAA Paper, to be presented at the 32th Fluid Dynamics Conference, St. Louis, 2002.

[32]Mack, L. M., "Boundary Layer Linear Stability Theory," Special Course on Stability and Transition of Laminar Flow, AGARD Report, 1984.

[33]Saric, W. S. and Reed, H. L., "Supersonic Laminar Flow Control on Swept Wings Using Distributed Roughness," AIAA Paper, 2002-0147, 2002.